

Cite this article as: Yin Jiaqing, Cui Shushan, Mo Wenlin, et al. Kinetics of Isothermal Transformation of U-2Nb Alloy[J]. Rare Metal Materials and Engineering, 2022, 51(12): 4508-4518.

ARTICLE

Kinetics of Isothermal Transformation of U-2Nb Alloy

Yin Jiaqing, Cui Shushan, Mo Wenlin, Rui Keqiang, He Shixiong, Chen Dong, Mo Chuan, Fa Tao

Institute of Materials, China Academy of Engineering Physics, Mianyang 621907, China

Abstract: The isothermal transformation kinetics of U-2Nb alloy was investigated. Based on metallographic quantitative measurements, the general kinetics was presented with the time-temperature-transformation (TTT) diagram. Results show that considerable discrepancies are identified in comparison with previous work on similar alloys. The differences are mainly attributed to two different transformation mechanisms, namely the monotectoid and the discontinuous precipitation reactions, which are operated at higher (550~647 °C) and lower (450~550 °C) temperatures, respectively. In addition, the growth rate of the acicular α precipitate in its lengthening direction, which proceeds through monotectoid reaction, was discussed. Modeling of the lengthening rate was carried out with the Zener-Hillert model supposing a diffusion-controlled mechanism.

Key words: U-Nb alloy; TTT diagram; isothermal transformation; kinetics

Uranium alloys is one of the potential metallic fuels for Gen-IV fast breeder reactors. Addition of alloy elements is necessary to ensure optimized properties upon functional conditions. Niobium is one of such optional elements and the U-Nb alloy has been persistently studied^[1-3]. Morphology of U-2Nb alloy (all in mass percent in this work unless otherwise specified) under isothermal transformation has been discussed in a preceding study^[4]. Below the monotectoid temperature of 647 °C^[5], as shown in Fig.1 (also reported to be 634 °C^[6]), it is found that the transformation may proceed through two different mechanisms, namely α precipitation (monotectoid reaction, α is the uranium-rich phase with niobium content less than about 0.08wt%) or discontinuous precipitation (DP, γ_1 (U-rich bcc) \rightarrow α (orth) + $\gamma_{1,2}$, where the $\gamma_{1,2}$ phase has composition between the γ_1 and γ_2 (U-depleted bcc, 54wt% Nb) phases). The monotectoid product is characterized with acicular morphology and is identified at higher temperatures of 550~635 °C. Partition of Nb from the depleted α phase to its surrounding γ phase is accomplished at the growing tip allowed by the high diffusion rate. In addition, at lower temperatures, the products are characterized with lamellar morphology where effective partition of Nb between the two lamellar phases is supposed to mainly occur within an interface ahead of the common growing front^[7]. In either case, the reactions mentioned above should both be classified into

the first stage of transformation since the composition of product γ phase is far lower than the equilibrium γ_2 given by the phase diagram (about 54wt% at room temperature^[5]), as shown in Fig. 1^[8]. With prolonging the isothermal holding time, the metastable $\gamma_{1,2}$ will continue to transform into final α + γ_2 mixture. In current alloy system, as stated by Jackson with similar alloy^[9], the first stage may complete within 1 h while the latter can take several days.

Transformation kinetics of uranium-based alloys under isothermal conditions were intensively studied in the period of 1960s~1970s. Howlett^[10] in 1963 constructed the time-temperature-transformation (TTT) diagram for U-6Mo alloy with metallography and hardness measurements. In the following year, Peterson et al^[11] surveyed series of uranium-based binaries and ternaries. For U-Nb binaries, TTT diagrams were constructed for alloys with Nb content of 5wt%, 8wt%, and 10wt%. In 1969, Castaldelli et al^[12] reported the TTT diagrams of U-2Nb and U-2Mo alloys. Jackson^[13] in 1971 published the isothermal transformation kinetics of U-5.5Nb alloy. Thereafter, Djuric^[14] investigated the isothermal decomposition behavior of U-9.5Nb alloy. It is found that the TTT diagrams of U-Nb system are well documented with Nb composition spanning from 2wt% to 10wt%. However, phase transformation of U-Nb alloys below the monotectoid temperature is rather complicated. The complexities were

Received date: December 27, 2021

Foundation item: National Natural Science Foundation of China (51901210, 21908210); CAEP Foundation (CX20210008)

Corresponding author: Fa Tao, Ph. D., Professor, Institute of Materials, China Academy of Engineering Physics, Mianyang 621907, P. R. China, Tel: 0086-816-3626767, E-mail: fatao@caep.cn

Copyright © 2022, Northwest Institute for Nonferrous Metal Research. Published by Science Press. All rights reserved.

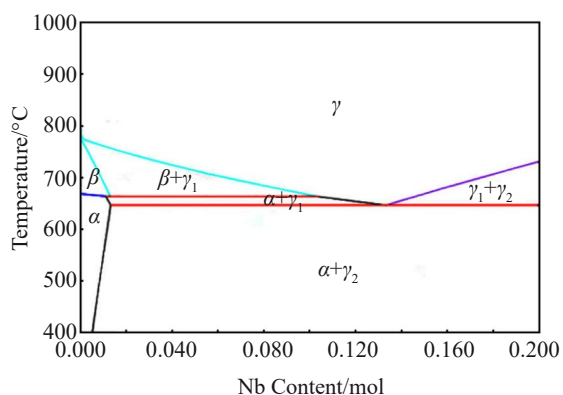


Fig.1 U-Nb phase diagram calculated with the Thermo-Calc software^[8] and the thermodynamic models of Duong^[5]

enounced recently^[7,15] owing to the advancement of experimental techniques, e. g. scanning electron microscopy (SEM), transmission electron microscopy (TEM), which allow observation at much higher resolution. For instance, the metallographic evidence of discontinuous coarsening (DC) in U-Nb system was identified until 2011 by Hackenberg et al^[14]. Moreover, the “general precipitation” occurring before the DP reaction was identified by SEM^[7] and in-situ synchrotron X-ray diffraction^[16] techniques, which was not shown in Jackson’s TTT diagram for U-6Nb alloy^[12]. Meanwhile, some other most advanced experimental resources for materials research were recently applied to study the transformation kinetics of uranium-based alloys^[17-19].

For U-2Nb alloy, to the best of our knowledge, systematic survey of the transformation kinetics under isothermal conditions was solely reported by Castaldelli et al^[11] below 647 °C, and they gave a continuous “C” curve down to about 400 °C. This is inconsistent with our recent findings that two different transformation mechanisms are operated in this temperature range^[4]. It should be further addressed that we thought that the monotectoid reaction identified in the U-2Nb alloy cannot fully coincide with the “general precipitation” (GP) recognized in the U-6Nb system^[7,15], as has been discussed in previous study^[4]. At least two different features can be clarified. Firstly, the size of α -U precipitates is relatively coarser in U-2Nb alloy when observation was taken at roughly the same temperature and holding time (Ref. [4] and Ref. [7]). Secondly, the monotectoid reaction was identified as competitor of DP reaction in U-2Nb system, while it was recognized as precursor of DP in U-6Nb system. Nevertheless, the differences mentioned above might originate from different amounts of driving force available for the two alloys, and thus the two terminologies may be simplified into one.

The current study aims to re-construct the TTT diagram of U-2Nb below the monotectoid temperature based on the recent understanding of microstructure reviewed above. Metallographic method was employed. The in-situ neutron diffraction technique may give a more precise determination of phase fraction; however, it is challengeable to choose a suitable cooling rate from a temperature in the γ -phase region

to the isothermal holding temperature for the neutron diffraction technique. Therefore, the transformation kinetics observed with traditional metallography method is still meaningful and will be presented.

1 Experiment

The nominal composition of the alloy studied in this work is U-2Nb. Samples were prepared through arc melting in a non-consumable electrode arc-melter. The inductively coupled plasma mass spectroscopy (ICP-MS) showed that after the melting, the samples have an average niobium content of 2.03%. Inclusion particles can be seen in the sample, mostly identified as U(C,N) and occasionally as Nb₂C. All samples were encapsulated with a quartz tube under vacuum (10^{-3} ~ 10^{-4} Pa) before subjecting to the isothermal holding. In order to eliminate the micro-segregation, all samples were initially normalized at 1000 °C for 12 h. Thereafter, isothermal holding in the temperature range of 550~635 °C was carried out by transferring the samples directly from the normalizing furnace into another muffle furnace preheated to the desired temperature. For lower temperature range of 450~500 °C, however, a different procedure was applied in consideration of influence of the martensite start temperature (M_s) during the cooling process, within 535~545 °C^[12]. Instead, samples were firstly water quenched from 1000 °C and then isothermally held in a preheated muffle furnace. Illustration of the isothermal holding procedure has been reported in previous studies^[3,4], which will not be reproduced here. After the isothermal holding, samples were sectioned followed by the standard metallographic procedure. Final polishing was implemented either with 1 μ m diamond or 0.05 μ m silica suspension regarding on light optical microscopy (OM) or scanning electron microscopy (SEM). Electropolishing was carried out with a 5% H₃PO₄ water solution operated at 3 V for 3~5 s. The morphology of the alloy was observed by a field emission gun-scanning electron microscope (FEG-SEM, 15 kV with a working distance of roughly 4 mm). The hardness test was implemented with Rockwell hardness criterion under HRC scale. For each test, the sample was Φ 10 mm \times 5 mm in size. The surface applied for test was initially ground with SiC paper up to #1000. For each test, three measurements were randomly taken after the calibration.

1.1 Measurement of general kinetics

Measurement of the fraction of transformation products was carried out through analysis on the OM microstructures. The images were firstly transferred into 8-bit gray-scale files and then analyzed with the MIAS-2000 software. The software allows analysis based on gray value of individual pixel. For each specimen, at least 10 images were analyzed. A special case is the measurement of specimen transformed at 550 °C, where both acicular and nodular (lamellar under SEM) structures are present. As shown in Fig.2a, growth rate of the nodular structure is generally much faster than that of the acicular structure. This leads to a larger volume of the former. Meanwhile, it is noticed that the gray values of the two

structures are different. Thus, measurement was made twice at 550 °C for each image. The first quantification was taken for all transformed structures and another one was then taken by adjusting the tolerance parameter for gray value in order to exclude the acicular structure with lower gray value (see the area marked by arrow in Fig.2a). Nevertheless, as can be seen in Fig. 2b, with prolonging the isothermal holding time, the acicular structure may impinge on the nodular structure, which makes it difficult to distinguish one structure from another.

Considerable uncertainty thus arises in quantification results obtained at 550 °C, especially for specimens with longer time of isothermal holding. For all measurements, analysis was carried out on micrographs taken from the same magnification, i.e. 100×. This criterion, however, causes some uncertainties in the quantification result. Fig. 3, for example, shows a case where initial austenite phase is still remained (the areas indicated by the arrows) but can only be identified at higher magnifications. Nonetheless, the criterion of the same magnification applied for all samples was strictly followed, and the quantification results will thus give a shorter time for the completion of transformation than it should be. Finally, it should be clarified that the transformed area quantified in current study actually corresponds to the two-phase mixture ($\alpha + \gamma_{1,2}$), which cannot be distinguished under OM.

1.2 Measurement of lengthening rate of acicular structure

For acicular α precipitates, the general kinetics is mainly controlled by nucleation and lengthening growth of the precipitates. Aaronson and Wells^[20] defined a group of closely packed plates with the same crystalline orientation as a sheaf of plates, and explained the morphology by sympathetic nucleation. The definition of the “sheaf” is accepted in current work. The longest sheaf in each OM image (a few SEM images were also applied) was taken as representative for specific specimen, i.e. it is supposed to be the length of the sheaf formed the earliest. For each specimen, at least 6 micrographs were analyzed (mostly 10 micrographs, except for microstructure transformed at 550 °C where the measurement was interfered by the DP structure and

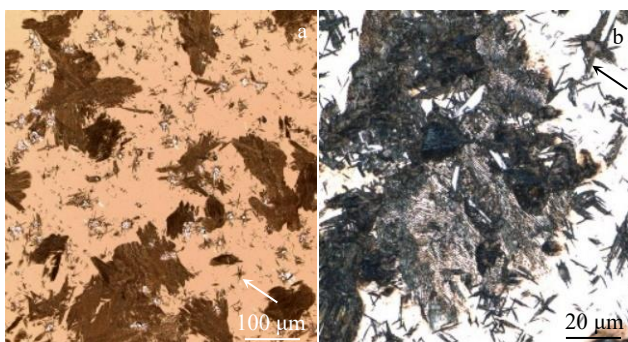


Fig.2 OM microstructures of specimen isothermally held at 550 °C for 3 min and interrupted by water quenching (arrows indicate acicular structure)

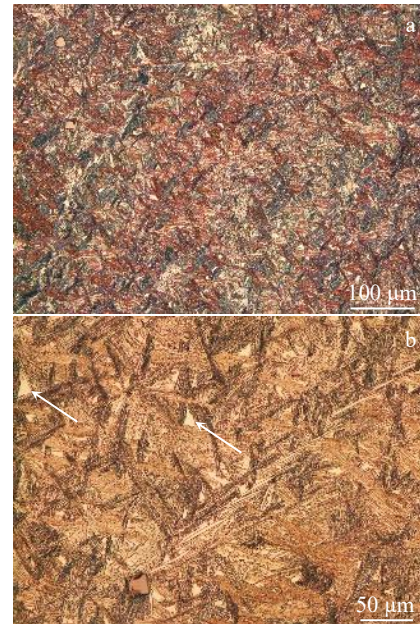


Fig.3 OM microstructures of specimen isothermally held at 635 °C for 1 h and water quenched (untransformed regions cannot be distinguished at lower magnification of Fig. 3a but can be identified at higher magnification of Fig. 3b, which are indicated by the white arrows)

it is difficult to locate a sheaf of acicular structure in its full length).

2 Results and Discussion

2.1 Microstructure

2.1.1 OM observation

Isothermal transformation at 635 °C leads to an acicular product nucleated at the grain boundaries and the inclusion/matrix interfaces, as shown in Fig. 4a. At higher magnifications, it is observed that each acicular structure consists of many parallel α precipitates with γ phase in-between. Similar structure is observed at 600 °C but with finer α precipitates (the fineness cannot be revealed by OM), as shown in Fig. 4b. With further decrease in holding temperature to 550 °C, apart from the acicular structure, a nodular or blocky structure is also observed, see Fig. 2. Isothermal holding of the quenched samples at 500 and 450 °C leads to the nodular product solely. A typical example is shown in Fig. 4c. It can be seen that the transformation at these two temperatures is influenced by the prior martensitic structure. The white martensite plates, as shown in Fig.4c, are remained until the late stage of transformation.

2.1.2 SEM observation

Both the acicular and the nodular structures are two-phase mixtures ($\alpha + \gamma_{1,2}$). At most temperatures in current study, inner structures of the samples cannot be distinguished by OM. As shown in Fig.5a and 5b, the SEM observation reveals that the acicular structure forms through the precipitation of α -phase. The primary interspace between two neighboring precipitates



Fig.4 Typical morphologies of transformation products taken from the samples after interrupted isothermal treatment: (a) 635 °C, 20 min; (b) 600 °C, 8.5 min; (c) 500 °C, 5 min

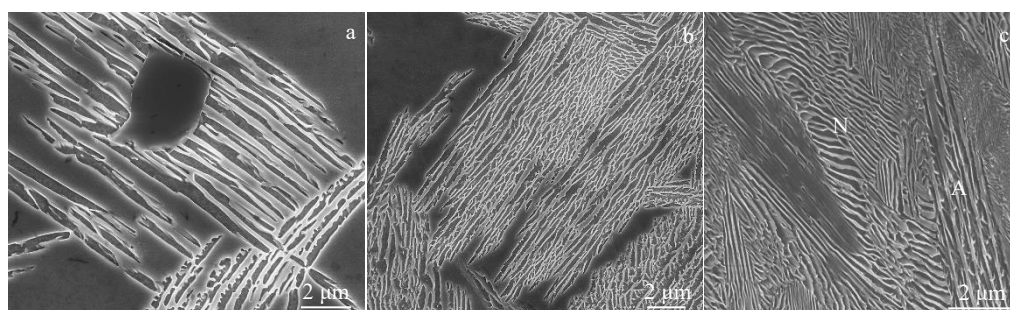


Fig.5 SEM morphologies of acicular (A) and nodular (N) structures of samples after isothermal holding under different conditions: (a) 635 °C, 8.5 min; (b) 600 °C, 10 min; (c) 550 °C, 3 min

is controlled by the nucleation rate at their nucleation sites. With decreasing the holding temperature, the driving force available for α precipitation (which is received in the cooling in the homogenization temperature) increases and thus the nucleation rate increases. It is thus expected that the acicular structure is much finer at lower temperatures and the chance to find an ideal acicular unit in its full length is small. Often, due the sectioning effect, the acicular structure is rather complicated, as shown in Fig.5b.

The volume of the γ_{1-2} phase is controlled by its Nb content receiving from the α -phase in vicinity. The nodular structure is formed through cooperative growth of the two phases with characteristic common growth front. In U-Nb system, it is well established that such lamellar structure corresponds to the “discontinuous reaction” mechanism^[15]. Existence of both

the acicular and nodular structure at 550 °C, shown in Fig.5c, suggests that both monotectoid reaction and discontinuous reaction can occur at this temperature. The nodular structure transformed at 500 and 450 °C is rather fine, which makes it difficult to reveal its inner morphology. Fig.6 shows that the growth front is lamellar. It is frequently observed that some prior martensite plates are remained inside the nodular colony.

2.2 General transformation kinetics

2.2.1 Experimental observation

The isothermal holding conditions investigated in current work are shown in Fig.7. Quantification results of mean value of the overall transformation fraction for some typical treatments are also presented correspondingly. It can be seen that a common C curve can be drawn for the start of transformation between 450~635 °C. The nose temperature is

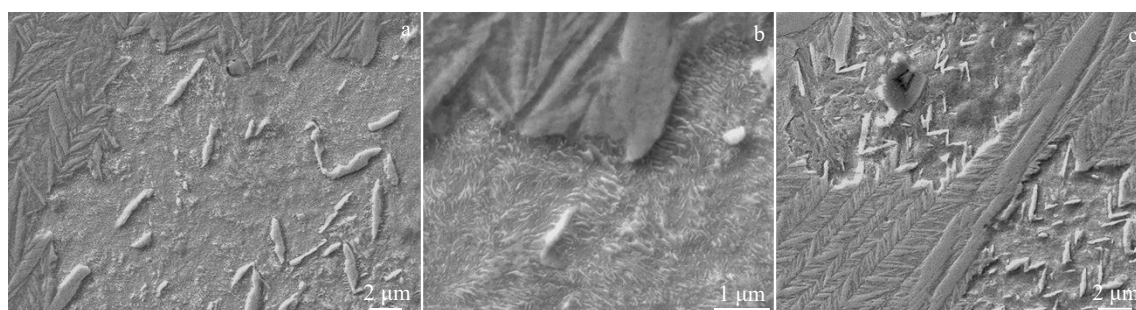


Fig.6 SEM morphologies of samples isothermally held below the M_s temperature: (a, b) 500 °C, 10 min; (c) 450 °C, 10 min

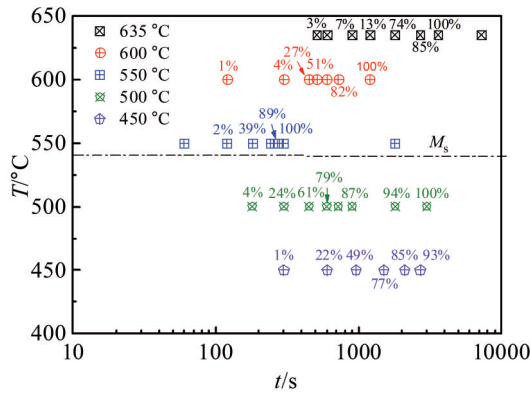


Fig.7 Isothermal holding conditions investigated in current work (notations of transformation fractions are made for some typical specimens, and the presented fractions for 550 °C here are overall fraction of transformation products)

around 550 °C, which is roughly in agreement with previous report (about 575 °C according to Ref. [12]). Results of hardness test are shown in Fig. 8. With increasing extent of decomposition of γ_1 , the overall hardness drops since the dual-phase products are weaker than the single parent γ_1 phase which was quenched into α' . The hardness decreases with prolonging isothermal holding time. The evaluated transformation start and finish time in such way generally agrees with metallographic observation (Fig.7). Generally, the higher the transformation temperature, the lower the hardness when transformation is completed. It is noticeable that the initial hardness is different between specimens isothermally held at 450~500 °C and 550~635 °C. This is attributed to the up-quenching method applied in the former temperature range while it is the downward-quenching in the latter.

2.2.2 KJMA fitting

The transformation kinetics under isothermal conditions is commonly fitted with the Kolmogorov-Johnson-Mehl-Avrami (KJMA, also quoted as JMA or Avrami) equation^[21], shown as

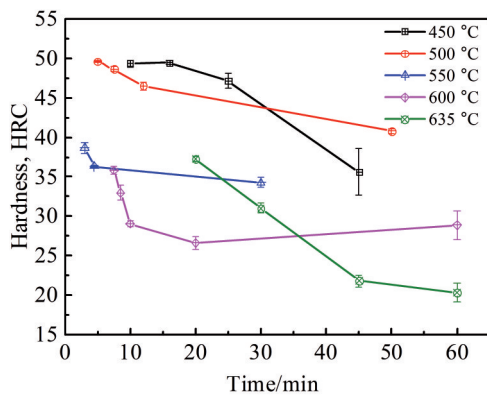


Fig.8 Results of Rockwell hardness test for specimens with various isothermal holding temperatures and time ended with water quenching (originally published in Ref. [3], modification is made in current version with some additional data)

follows,

$$f=1-\exp(-kt^n) \tag{1}$$

where f is the transformation fraction, n is an exponential constant independent of temperature under the same nucleation mechanism, k is a parameter sensitive to temperature and is influenced by both nucleation and growth behavior^[22].

With experimental data of transformation fraction presented in previous section, the two parameters, k and n , in Eq.(1) can be obtained through linear fitting under logarithm plot. Table 1 lists the obtained fitting parameters for transformation at five investigated temperatures. Specifically, the transformation fractions of the nodular and the acicular structures which are both presented at 550 °C are now separately treated. It is seen that the exponential parameter n for nodular structure varies roughly between 2.4~2.7, while it is within 3.2~3.7 for acicular structure. Christian^[23] made a systematic interpretation for various values of parameter n . According to the interpretation, a value of 3 for discontinuous precipitation implies saturation of nucleation sites. For diffusion-controlled growth, on the other hand, a value of n over 2.5 represents an increasing nucleation rate. In either case, the high value of n implies a high nucleation rate, e.g. intragranular nucleation, is functioned in a considerable extent.

Referring to the metallographic observation in preceding work^[4], inclusion particles are frequently seen in every sample, which are definitely contributed as nucleation sites. Moreover, the large grain size, usually in hundreds of microns, results in fewer grain boundaries available for nucleation. It thus seems reasonable for the high value of n obtained in current work. It should be mentioned that Eckelmeyer^[24] studied the DP transformation kinetics in U-4.5Nb alloy, and obtained values of n varying from 1 up to 3. More recent works by Hackenberg^[15] and Zhang^[16] on DP reaction in U-Nb alloys with niobium content of 5.5wt%~7.4wt% all showed n value around 1.

The fitting curves with KJMA equation at various temperatures together with raw data are shown in Fig.9 and Fig. 10. It is seen that the “S” shape of fitting curve is reasonable at all temperatures except 550 °C regarding on the overall transformation fraction (Fig. 10). This is because the overall transformation fraction at this temperature is simply

Table 1 Fitting parameters of KJMA equation obtained at specific isothermal holding temperatures (DP and GP refer to discontinuous precipitation and general precipitation, respectively)

$T/^\circ\text{C}$	Microstructure characters	Transformation mechanism	$\ln k$	n
450	Nodular	DP	17.5±2.7	2.4±0.4
500	Nodular	DP	15.5±2.0	2.4±0.3
550	Nodular	DP	14.8±4.7	2.7±0.9
550	Acicular	Monotectoid/GP	19.3±1.7	3.2±0.3
600	Acicular	Monotectoid/GP	23.4±6.5	3.7±1.0
635	Acicular	Monotectoid/GP	24.6±5.1	3.6±0.7

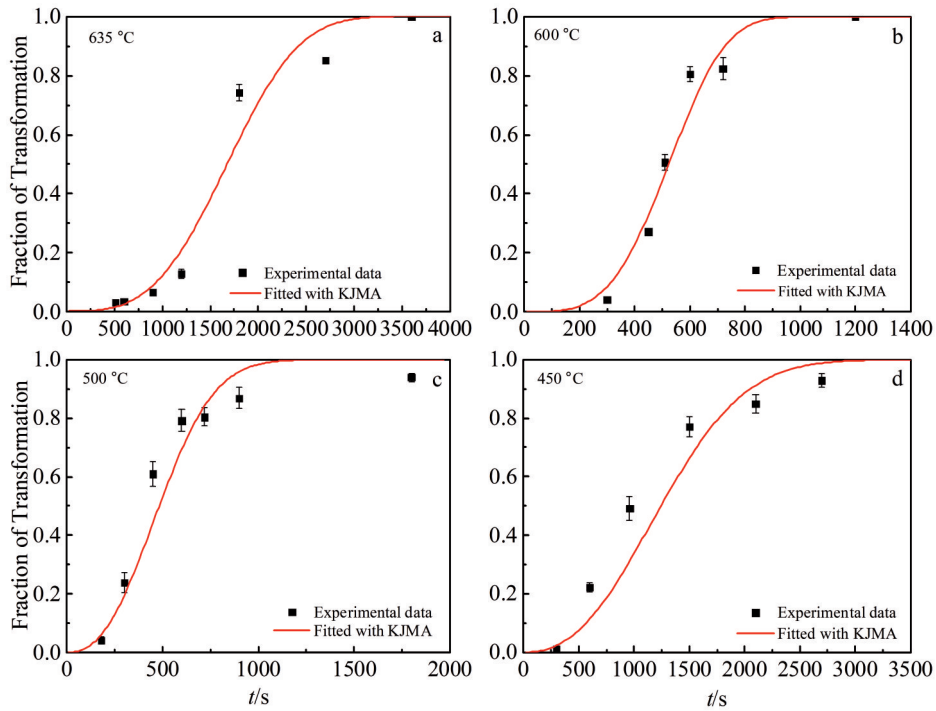


Fig.9 Fitting curves with KJMA equation in comparison with raw experimental data for transformation fraction with isothermal holding at specific temperatures: (a) 635 °C, (b) 600 °C, (c) 500 °C, and (d) 450 °C

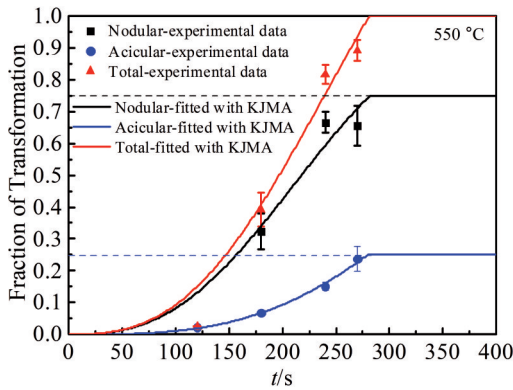


Fig.10 Fitting curves with KJMA equation in comparison with raw experimental data for transformation fraction with isothermal holding at 550 °C (total fraction was evaluated simply by summing the fractions of nodular and acicular structures, and the dash lines are set at fraction values of 0.25 and 0.75 for the limit fraction for acicular and nodular structures, respectively)

taken as the sum of both kinds of structures without taking into account of some important factors. Firstly, incubation time of two kinds of structures should be different; the nodular structure is not observed in early stage of transformation but is supposed to present as early as the formation of acicular structure in the calculation. Secondly, in the later stage of transformation, growth of two kinds of structures will compete with each other, which will slow down the growth

kinetics, and this effect is also neglected. Therefore, the overall fraction is overestimated to some extent by two ends of the curve at 550 °C.

As already shown in Fig.7, the nose temperature is roughly around 550 °C. Below this temperature, the growth process is mainly controlled by the diffusion rate of Nb, which is a thermally activated process. The reaction rate in this temperature range will thus follow an Arrhenius expression. Considering that the extent of reaction can be expressed as certain fractions varying from 0 to 1, the expression can be formulated as follows,

$$t_f = A \exp[(-Q_A)/RT] \tag{2}$$

where t_f is the reaction time to reach certain transformation fraction, A is reaction constant, Q_A is the apparent activation energy, R is the gas constant, and T is the absolute temperature. Taking natural logarithms on the two sides of Eq.(2):

$$\ln t_f = \ln A - \frac{Q_A}{RT} \tag{3}$$

For a given fraction value, one can thus evaluate the apparent activation energy with Eq.(3). Plotting of $\ln t_f$ versus $1/T$ gives a slope in value of Q_A/R . As shown in Fig.11, it can be seen that for several chosen transformation fractions, the values of slope are quite close. The mean activation energy was evaluated to be 87 kJ·mol⁻¹, smaller than the value needed for volume diffusion of niobium in γ phase which is 137 kJ·mol⁻¹ referring to Peterson and Ogilvie^[25]. As discussed earlier, this can be explained by the interface diffusion which is supposed to be more effective in DP reaction.

Table 2 compares the apparent activation energy for general

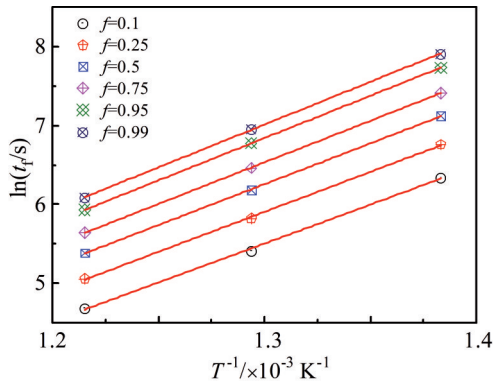


Fig.11 Arrhenius plots of KJMA model for specific transformation fractions

transformation kinetics of U-Nb alloys evaluated with KJMA fitting method. It can be seen that there is considerable discrepancy between the current work and previous reports. Hackenberg et al^[7] speculated higher Q_d value in comparison to that of bulk diffusion due to the possible contribution from nucleation process. Another clue might be the chemical composition which influences the driving force for the growth process, though the tendency is ambiguous with the information shown in Table 2. Further information on the general kinetics, especially for similar alloy compositions and isothermal holding temperatures, is needed to justify the speculations mentioned above.

2.2.3 TTT diagram

TTT diagrams are usually given in “C” curves for specific fractions. With the fitting parameters of KJMA equation established in previous section, the reaction time to reach transformation fraction of 1%, 50%, and 99% was calculated at the five temperatures. The C-curves were thereafter constructed by fitting these calculated data points, as shown in Fig.12. Two C-curves are now constructed in consideration of two fundamentally different transformation mechanisms, i. e., the monotectoid reaction and the discontinuous precipitation. The monotectoid reaction in current work is in terminology of invariant reaction which differs from the discontinuous reactions^[26]. Moreover, it should be emphasized that the TTT diagram constructed here is for the first stage of transformation discussed in the introduction section, i. e., $\gamma_1(\alpha') \rightarrow \alpha + \gamma_{1,2}$.

Table 2 Apparent activation energy (Q_A) of general transformation kinetics for U-Nb alloys evaluated with KJMA fitting method

Alloy	Temperature range/°C	Q_A /kJ·mol ⁻¹	Ref.
U-4.5Nb	350~390	209	[24]
U-5.5Nb	300~500	156±20	[15]
U-5.5Nb	300~625	137±15	[7]
U-7.5Nb	300~450	168±15	[7]
U-2Nb	450~550	87±2	This work

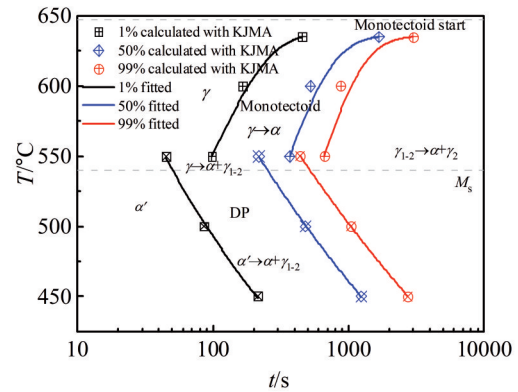


Fig.12 TTT diagram for U-2Nb constructed through KJMA equation

The TTT diagram constructed in current study is compared to the work by Castaldelli et al^[12]. Apart from the difference of separated C curves in current work, it is seen that above the Martensite start temperature, the transformation kinetics determined in current work is much slower, e. g., about two orders of magnitude than that reported by Castaldelli et al at 550 °C. The M_s temperature determined in current work is 535~540 °C, roughly in agreement with Castaldelli et al's work^[12]. We noticed that lead bath was used by Castaldelli et al for isothermal holding, while in current work samples were transferred from one furnace to another. However, it is still difficult to reconcile the big difference in kinetics by considering the experimental details solely. Meanwhile, with U-2.4Nb alloy, Jackson^[9] mentioned that the C-curve has a nose at 570 °C, where “the first decomposition starts in about one minute and is complete in about one hour”. As demonstrated in Fig.13, Jackson's observation is in reasonable agreement with current work. Finally, it should be added that a recent work by Zhang et al^[16] showed that for U-6Nb alloy characterized by in-situ synchrotron X-ray diffraction technique, the first stage of transformation takes about 13 min for completion at 565 °C and 23 min at around 530 °C. Thus the kinetics of isothermal decomposition for the two U-Nb alloys seems the same order of magnitude despite of morphological differences of products as claimed in the introduction section.

One may notice that the two “C” curves presented in current work are incomplete (e. g., the acicular structure should form at temperature lower than 550 °C). Therefore, additional isothermal treatments at 500 °C are conducted to investigate the transformation behavior when the samples are transferred directly from 1000 °C to 500 °C. Unfortunately, since the samples are encapsulated in the quartz tube (for safety and oxidation concerns), it appears that the quenching rate is not fast enough to exclude the microstructure transformed in the temperature range around 550 °C under cooling. A more complete and accurate TTT diagram of U-2Nb system thus remains for future work which requires capable experimental equipment to allow sufficient cooling rate.

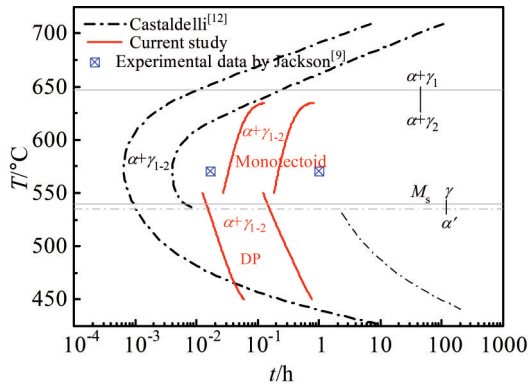


Fig.13 Comparison of TTT diagrams for U-2Nb in current study with previous report

2.3 Lengthening rate of acicular structure

2.3.1 Experimental measurement

Acicular structure is commonly observed in many alloy systems. It is well established that the growth of individual plate within the structure is limited by semi-coherent interfaces in its widening and thickening directions^[21]. In addition, the lengthening rate is of particular interesting since it involves a fundamental issue of partitioning of alloy elements during the growth process. Such partitioning between the parent and product phases is supposed to be the controlling factor of growth rate for the acicular unit. As already introduced earlier, the longest length of the general acicular structure among several measurements was taken as representative length of individual unit due to the fineness of the microstructure (50~600 nm^[4]). Results of measurement are shown in Fig. 14 and Fig. 15. Under isothermal holding, a constant lengthening rate is expected. Linear fit of the data

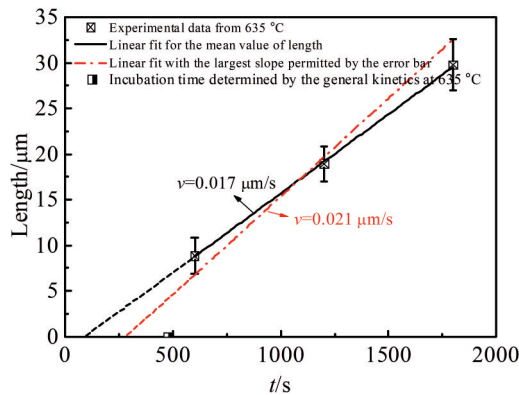


Fig.14 Lengthening rate evaluated through linear fitting of the longest length obtained for specimens isothermally held at 635 °C for different time (solid line with least squares method, dash-dot line for the largest slope permitted by the error bar of experimental data; extrapolation of fitting lines to zero of length was made in dash line to evaluate the incubation time, which is in comparison with the value predicted by the general kinetics of acicular structure)

gives a lengthening rate of 0.017 μm/s at 635 °C, as shown in Fig.14. The fitting line is extrapolated to the abscissa, i.e. dash line in the figure, by which the incubation time is determined roughly as 100 s. This value differs far from the incubation time determined by the general kinetics which has been discussed in preceding section. Another fitting attempt was thus made to obtain a larger slope allowed by the error bar of experimental data. However, the lengthening rate only changes slightly to 0.021 μm/s. Similar treatments were carried out for lengthening growth under isothermal holding at 600 and 550 °C, as shown in Fig. 15. It is seen that the lengthening rates determined at these two temperatures are rather close, which are one order of magnitude faster than the value obtained at 635 °C. It is well established that the lengthening rate is mainly controlled by the driving force available for the growth process and the diffusion rate of solute element. Interplay of the above two factors will result in a “C” curve as a function of reaction temperature. It seems that the lengthening rate approaches the maximum at the nose temperature adjacent to 550 °C. This speculation will be further investigated in the following section.

2.3.2 Modelling of lengthening rate

Diffusion-controlled model of lengthening rate of acicular unit is initially proposed by Zener^[27]. His model was later modified by Hillert^[28], which is often referred as Zener-Hillert model. A latest version of the model has been reported^[29] with an expression as follows:

$$v = \frac{D\Delta G_m^0/V_m}{2\sigma^{\alpha\gamma}} \cdot \frac{x^{\gamma/\alpha} - x^0}{x^0 - x^{\alpha/\gamma}} \cdot \frac{\rho_{cr}}{\rho} \quad (4)$$

where D is the diffusion coefficient, ΔG_m^0 is the total driving force for precipitation, V_m is the molar volume of precipitate phase (α), $\sigma^{\alpha\gamma}$ is the interfacial energy, $\sigma^{\alpha/\gamma}$ and $\sigma^{\alpha/\alpha}$ are the mole fractions of solute in γ and α at the interface, respectively, x^0 is the original alloy composition, ρ_{cr} and ρ are the critical and actual radius of curvature of the plate tip, respectively. The

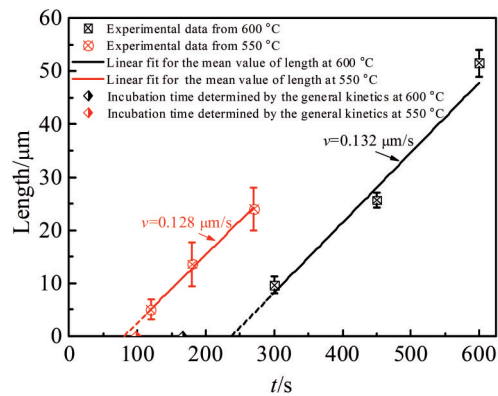


Fig.15 Lengthening rate evaluated through linear fitting of the longest length obtained for specimens isothermally held at 600 °C and 550 °C for different time (solid line with least squares method; extrapolation of fitting lines to zero of length was made in dash line to evaluate the incubation time, which is in comparison with the value predicted by the general kinetics of acicular structure)

critical radius is defined at which the growth rate is zero.

Obviously, the theoretical growth rate will vary with the actual radius, which is an unknown quantity. Zener^[27] proposed that the maximum growth rate is preferred by the nature when the actual radius is adjusted to an optimal value. In Hillert's earlier treatment^[28], this value was fixed to be $\rho = 2\rho_{cr}$. The latest treatment, as shown in Eq.(4), allows the ρ_{cr}/ρ to be set as a variable, and this in turn affects the capillarity effect and thus the local equilibrium. The crucial step is to find the $x^{\gamma/\alpha}$ for a certain value of ρ_{cr}/ρ . Firstly, the active driving force, ΔG_m , can be evaluated with the following equation:

$$\Delta G_m = (1 - \rho_{cr}/\rho) \Delta G_m^0 \quad (5)$$

The $x^{\gamma/\alpha}$ can be obtained by drawing a local equilibrium tie-line in a molar Gibbs energy diagram at given temperatures.

Fig.16 is given as an example to demonstrate how the $x^{\gamma/\alpha}$ is calculated for each value of ρ_{cr}/ρ at a specific temperature. The molar Gibbs energy curves were calculated with the recent reassessed thermodynamic model for U-Nb system by Duong et al^[5]. It can be seen that curve for γ phase shows double-well shape. This shape might result in more than one cross point given by the local equilibrium tie-line and the molar Gibbs energy curve, i. e. G_γ in Fig. 16. In such circumstances, the lowest value of $x^{\gamma/\alpha}$ is adopted.

For now, the remaining unknown quantities in Eq. (4) are $x^{\gamma/\alpha}$, $\sigma^{\alpha\gamma}$, V_m , and D . It is well established that the chemical content of α phase is close to the equilibrium. The $x^{\alpha/\gamma}$ is thus set as 0.002 for all calculations in current work. Experimental information of the interfacial energy, $\sigma^{\alpha\gamma}$, is absent in literatures for U-Nb system. Hackenberg et al^[15] tried to evaluate the value with the Becker equation^[30], which gives a value in the range of 100~150 mJ/m² regarding on the Nb content in the γ phase, i.e. $x^{\gamma/\alpha}$. It should be pointed out that the above evaluation is carried out for DP reaction. One can

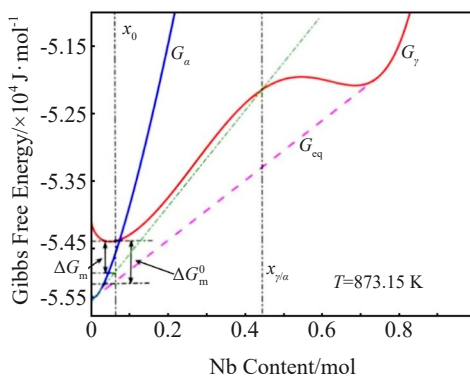


Fig.16 Molar Gibbs energy curves of orthorhombic (α) and bcc (γ) phases for U-Nb system as a function of mole fraction of niobium (calculation was conducted at 600 °C with thermodynamic model optimized by Duong^[5]; construction of local equilibrium tie-line, shown in dash-dot line and in green color for colored version, was made to locate the alloy content at the interface ($x^{\gamma/\alpha}$), which is determined accordingly by the active driving force, ΔG_m)

expect that in an early stage of α precipitation reaction, the $x^{\gamma/\alpha}$ should have a lower value, corresponding to a lower value of $\sigma^{\alpha\gamma}$. Notwithstanding, for simplicity, the $\sigma^{\alpha\gamma}$ is artificially fixed as 140 mJ/m² in this work. The molar volume is calculated with the formula proposed by Turchi^[31]. The expression is as follows:

$$V_m = x_{Nb}(1 + \alpha_{Nb}T)^3 V_m^{Nb} + (1 - x_{Nb})(1 + \alpha_U T)^3 V_m^U + \sum_{n \geq 1} a_n (x_{Nb})^n \quad (6)$$

where x_{Nb} is the mole fraction of Nb; V_m^{Nb} and V_m^U are the molar volume of pure Nb and U, with value of 10.83 and 12.89 cm³/mol, respectively. The constants in Eq.(7) are $\alpha_{Nb} = 7.3 \times 10^{-6} \text{ K}^{-1}$, $\alpha_U = 13.9 \times 10^{-6} \text{ K}^{-1}$, $\alpha_1 = 0.490347$, $\alpha_2 = -0.616518$, $\alpha_3 = 0.909831$, $\alpha_4 = -2.62558$, $\alpha_5 = 2.675619$, $\alpha_6 = -0.833959$.

Lastly, the diffusion coefficient of Nb in γ -uranium, D , is yet well documented so far. Due to the high temperature range of single γ -phase region in U-Nb system, experimental data are determined above the monotectoid temperature. Extrapolation to low temperature is commonly made based on the following formula:

$$D = D_0 e^{-Q/RT} \quad (7)$$

where R is diffusion rate constant, Q is the activation energy, R is the gas constant and T is the absolute temperature. Peterson and Ogilvie^[25] reported that for U-6Nb system, the D_0 and Q are $1.38 \times 10^{-8} \text{ m}^2/\text{s}$ and 136.4 kJ/mol, respectively. One can expect that the diffusion coefficient is not only temperature dependent but also as a function of Nb content. Fedorov et al^[32,33] published a series of tracer diffusivities for uranium alloys with Nb content spanning from 0at% to 100at%. Their results showed that with increasing the Nb content, the diffusion coefficient decreases. Applying the CAIPHAD method, Liu et al^[34] reported the optimized model for atomic mobilities of U- X alloys ($X = \text{Nb, Ti, Mo}$). Recently, the atomic mobilities for U- X binary system ($X = \text{Nb, Ti, Zr}$) were reassessed by Bian et al^[35]. In order to calculate the interdiffusion coefficient of Nb in γ phase as a function of both temperature and Nb content, the evaluation of atomic mobility for U-Nb system by Bian et al, which was coupled to the thermodynamic model described by Duong et al^[5], was adopted in current work.

Supposing a gradient of Nb across the α/γ interface, three kinds of diffusivities can be considered. The first one, D_b , calculated with the bulk Nb content, another type, D_{min} , calculated with the estimated $x^{\gamma/\alpha}$, and finally the effective diffusivity integrated through the whole interface referring to Trivedi and Pound^[36], D_{eff} ,

$$D_{eff} = \frac{1}{x^{\gamma/\alpha} - x^0} \int_{x^0}^{x^{\gamma/\alpha}} D(x) dx \quad (8)$$

The modelling results are shown in Fig.17 and Fig.18. As shown in Fig.17, the diffusivity with the bulk composition is considered, and the optimal radius varies with temperature. At 635 °C, the optimal ratio of ρ/ρ_{cr} is around 2 while it is over 4 at 550 °C. The maximum lengthening rate as a function of temperature, as well as specific choice of diffusivity, is shown in Fig.18. It can be seen that the calculated lengthening rates are lower than the experimental values, even as the maximum

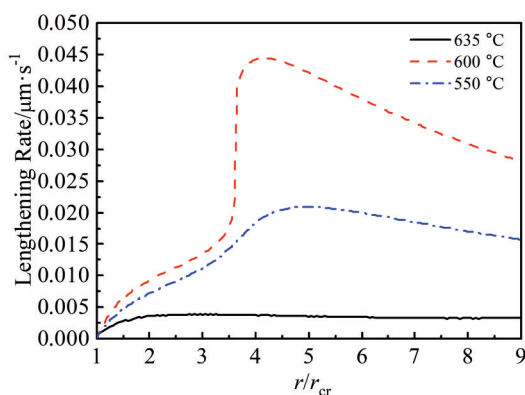


Fig.17 Lengthening rate varying with the ratio between the actual and critical radius of the tip of one acicular unit (the maximum lengthening rate is supposed to be given by the optimal ratio; diffusivity of D_b is applied)

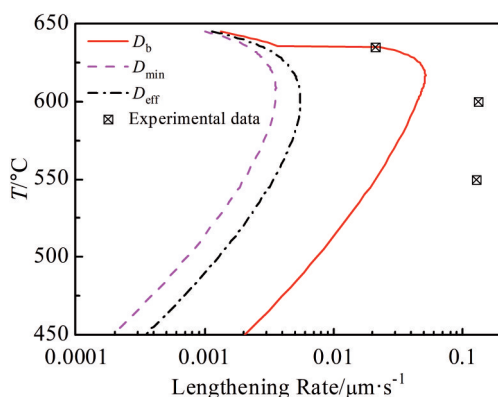


Fig.18 Lengthening rate of C curves calculated with different choices of diffusivities

diffusivity is applied (solid line in Fig.18). This discrepancy is much larger as the other two diffusivities are considered, as the maximum difference by a factor of about two orders of magnitude. Nevertheless, the discrepancy between the solid line and the experimental values is supposed to be acceptable. It is also noticed that the nose temperature of the C-curve of lengthening rate given by the modeling is around 620 °C, which is higher than the nose temperature given by the experimental data. Uncertainties of the modelling may be attributed to at least three factors. Firstly, the interfacial energy, $\sigma^{\alpha/\beta}$, is an unknown quantity in U-Nb system and is artificially fixed to a certain value in current modelling. Secondly, the atomic mobilities, which are adopted from literature, are optimized by experimental information in higher temperature range (800~2000 °C^[35]). Finally, the composition of Nb at the interface, $x^{\alpha/\beta}$, is assumed to be controlled by the active driving force, which is allowed to vary freely with different ratios of ρ/ρ_{cr} . These assumption may lead to a large value of $x^{\alpha/\beta}$, which is perhaps unrealistic since the actual distribution of Nb should be limited by the diffusion process. In general, it is safe to conclude that the lengthening growth of acicular unit by α precipitation in U-2Nb system can be satisfactorily described with a diffusion-

controlled model.

3 Conclusions

1) The transformation kinetics of U-2Nb alloy under isothermal treatment is investigated with metallographic quantitative measurements. Two kinds of structures, acicular and nodular corresponding to monotectoid and discontinuous precipitation reactions, respectively, are distinguished during the measurement. The general kinetics is analyzed through fitting the transformed fractions with the KJMA equation. The TTT diagram is then constructed which shows considerable discrepancy in comparison to the previous report. In particular, the lengthening kinetics of acicular structure is discussed by experimental and theoretical approaches.

2) By assuming a diffusion-controlled mechanism, modeling of the lengthening rate is implemented with the latest version of Zener-Hillert model, which allows searching of the optimal radius of acicular structure at the tip in order to generate a maximum growth rate. Three kinds of diffusivities of Nb that are coupled with thermodynamic factor are considered. The diffusion-controlled model can well predict the lengthening rate of α acicular precipitates in the U-2Nb system, despite of a considerable discrepancy in comparison to experimental values due to the uncertainties imported from several parameters applied in the model.

References

- 1 Wang Xiaoyin, Yang Jianxiong, Lang Dingmu et al. *Rare Metal Materials and Engineering*[J], 2008, 37: 1396 (in Chinese)
- 2 Chen Dong, Li Ruiwen, Ma Rong et al. *Rare Metal Materials and Engineering*[J], 2019, 48: 165 (in Chinese)
- 3 Rui Keqiang, Yin Jiaqing, Mo Wenlin et al. *Rare Metal Materials and Engineering*[J], 2021, 50(1): 271 (in Chinese)
- 4 Yin J, Wu M, Liao Y et al. *Journal of Nuclear Materials*[J], 2020, 540: 1
- 5 Duong T C, Hackenberg R E, Landa A et al. *Calphad*[J], 2016, 55: 219
- 6 Mo C, Mo W, Zhou P et al. *Journal of Materials Science & Technology*[J], 2021, 81: 229
- 7 Hackenberg R E, Emigh M G, Kelly A M et al. *The Surprising Occurrence of Non-steady-state Growth of Divergent Lamellar Decomposition Products in Uranium-Niobium Alloys: A Preliminary Report*[R]. US: Los Alamos National Laboratory, 2012
- 8 Andersson J O, Helander T, Höglund L et al. *Calphad*[J], 2002, 26: 273
- 9 Jackson R J. *Mechanical Properties of Continuously Cooled Uranium-2.4 Weight Percent Niobium Alloy*[R]. Colorado: Rocky Flats Plant, 1981
- 10 Howlett R W, Eycott A J, Kang I K et al. *Journal of Nuclear Materials*[J], 1963, 9: 143
- 11 Peterson C A W, Steele W J, DiGiallonardo S L. *Isothermal Transformation Study of Some Uranium-Base Alloys*[R]. California: University of California, 1964

- 12 Castaldelli L, Fizzotti C, Gandini A G. *Processes of Transformation in Alloys of Uranium Containing 2% Molybdenum and 2% Niobium*[R]. Italy: CNEN, 1969
- 13 Jackson R J. *Isothermal Transformations of Uranium-13 Atomic Percent Niobium*[R]. Colorado: Rocky Flats Golden, 1971
- 14 Djuric B. *Journal of Nuclear Materials*[J], 1972, 44: 207
- 15 Hackenberg R E, Volz H M, Papin P A et al. *Solid State Phenomena*[J], 2011, 172-174: 555
- 16 Zhang J, Brown D W, Clausen B et al. *Metallurgical and Materials Transactions A*[J], 2019, 50A: 2619
- 17 Steiner M A, Calhoun C A, Klein R W et al. *Journal of Nuclear Materials*[J], 2016, 477: 149
- 18 Brown D W, Bourke M A M, Clarke A J et al. *Journal of Nuclear Materials*[J], 2016, 481: 164
- 19 Zhang J, Hackenberg R E, Watkins E B et al. *Journal of Nuclear Materials*[J], 2020, 542: 1
- 20 Aaronson H I, Wells C. *Transactions of the AIME*[J], 1956, 206: 1216
- 21 Borgenstam A, Hillert M. *Phase Transformation in Steels*[M]. Cambridge: Woodhead Publishing, 2012
- 22 Porter D A, Easterling K E, Sherif M Y. *Phase Transformations in Metals and Alloys*[M]. UK: Taylor & Francis Group, 2009
- 23 Christian J W. *Theory of Transformations in Metals & Alloys* [M]. Oxford: Elsevier Science, 2002: 529
- 24 Eckelmeyer K H. *Physical Metallurgy of Uranium Alloys*[C]. Colorado: Sandia Labs, 1974: 427
- 25 Peterson N L, Ogilvie R E. *Transactions of the AIME*[J], 1963, 227: 1083
- 26 Manna I, Pabi S K, Gust W. *International Materials Reviews*[J], 2001, 46: 53
- 27 Zener C. *AIME*[J], 1946, 167: 550
- 28 Hillert M. *Jernkontorets Annaler*[J], 1957, 147: 757
- 29 Leach L, Hillert M, Borgenstam A. *Metallurgical and Materials Transactions A*[J], 2016, 47A: 19
- 30 Becker R. *Annals of Physics*[J], 1938, 32: 128
- 31 Turchi P. *Thermodynamic, Kinetic, and Physical Properties of Nb-U (Niobium-Uranium)* [R]. California: Lawrence Livermore National Laboratory, 2018
- 32 Fedorov G B, Smirnov E A, Gusev V N. *Atomic Energy*[J], 1969, 27: 864
- 33 Fedorov G B, Smirnov E A, Gusev V N. *Atomic Energy*[J], 1972, 32: 8
- 34 Liu Y, Yu D, Du Y et al. *Calphad*[J], 2012, 37: 49
- 35 Bian B, Zhou P, Wen S et al. *Calphad*[J], 2018, 61: 85
- 36 Trivedi R, Pound G M. *Journal of Applied Physics*[J], 1967, 38: 3569

U-2Nb 合金等温相转变动力学

尹嘉清, 崔书山, 莫文林, 芮克强, 何世雄, 陈冬, 莫川, 法涛
(中国工程物理研究院材料研究所, 四川 绵阳 621907)

摘要: 讨论了U-2Nb合金的等温转变动力学行为。通过金相定量测量, 构建了其宏观动力学曲线, 即时间-温度-相转变(TTT)曲线。对比之前在类似合金上的工作, 发现了较大的差异。该差异主要归因于2种不同的相转变机制, 即单析出反应和不连续析出反应, 它们分别在较高温度(550~647 °C)和较低温度范围(450~550 °C)下发生。此外, 讨论了通过单析出反应进行的针状 α 析出物在其长度方向上的生长速率。最后, 运用Zener-Hillert模型模拟了单析出反应受扩散控制时的生长速率并与实验数据进行了对比。

关键词: 铀铌合金; TTT图; 等温相转变; 动力学

作者简介: 尹嘉清, 男, 1989年生, 博士, 副研究员, 中国工程物理研究院材料研究所, 四川 绵阳 621907, 电话: 0816-3626767, E-mail: jiaqingyin@caep.cn